Pflugers Arch - Eur J Physiol (2008) 455:873–884
DOI 10.1007/s00424-007-0344-x

CELL AND MOLECULAR PHYSIOLOGY

Ca^{2+}/CaM-dependent inactivation of the skeletal muscle L-type Ca^{2+} channel ($Ca_v1.1$)

Katarina Stroffekova

Received: 29 June 2007 / Accepted: 5 September 2007 / Published online: 26 September 2007
© Springer-Verlag 2007

Abstract Ca^{2+}-dependent modulation via calmodulin (CaM) has been documented for most high-voltage-activated Ca^{2+} channels, but whether the skeletal muscle L-type channel ($Ca_v1.1$) exhibits this property has been unknown. In this paper, whole-cell current and fluorescent resonance energy transfer (FRET) recordings were obtained from cultured mouse myotubes to test for potential involvement of CaM in function of $Ca_v1.1$. When prolonged depolarization (800 ms) was used to evoke $Ca_v1.1$ currents in normal myotubes, the fraction of current remaining at the end of the pulse displayed classic signs of Ca^{2+}-dependent inactivation (CDI), including U-shaped voltage dependence, maximal inactivation (~30%) at potentials eliciting maximal inward current, and virtual elimination of inactivation when Ba^{2+} replaced external Ca^{2+} or when 10 mM BAPTA was included in the pipette solution. Furthermore, CDI was virtually eliminated (from 30 to 8%) in normal myotubes overexpressing mutant CaM (CaM_{1234}) that does not bind Ca^{2+}, whereas CDI was unaltered in myotubes overexpressing wild-type CaM (CaM_{wt}). In addition, a significant FRET signal (E=4.06%) was detected between fluorescently tagged $Ca_v1.1$ and CaM_{wt} coexpressed in dysgenic myotubes, demonstrating for the first time that these two proteins associate in vivo. These findings show that CaM associates with and modulates $Ca_v1.1$.

Keywords Ca_v1 channels · Skeletal muscle · Calmodulin · FRET · Ca^{2+}-dependent inactivation

Introduction

The skeletal muscle L-type Ca^{2+} channel ($Ca_v1.1$) is localized in regions of the T-tubular membrane that are closely apposed to the sarcoplasmic reticulum (i.e., the T-SR junction), and the primary role of $Ca_v1.1$ is to serve as the voltage sensor for skeletal muscle-type excitation–contraction (EC) coupling [20, 23, 45]. While Ca^{2+} currents through other L-type channels ($Ca_v1.2$, $Ca_v1.3$, and $Ca_v1.4$) have fairly well-understood physiological roles, the functional significance of Ca^{2+} current through $Ca_v1.1$ has remained uncertain [29, 33, 34, 44, 58]. This uncertainty stems from the fact that during single twitches of skeletal muscle fibers, fewer than 5% of $Ca_v1.1$ channels are thought to function as calcium channels, and twitches proceed normally in the absence of external Ca^{2+} [1, 2, 53]. However, some evidence indicates that Ca^{2+} entry through $Ca_v1.1$ may have significance for the long-term function of skeletal muscle. For example, it has been suggested that during sustained contractile activity, the presence of external Ca^{2+} and its flux through $Ca_v1.1$ contributes to maintaining contractile force [30, 46]. It has also been suggested that, in aged mammalian skeletal muscle, Ca^{2+} current through $Ca_v1.1$ may play a role in the mechanism of EC coupling and in sustaining contractile force [12, 36].

Dynamic changes in intracellular Ca^{2+} concentration ($[Ca^{2+}]_i$) are often the direct result of electrical signals in cells. It is now clear that many ion channels are subject to feedback modulation by changes in $[Ca^{2+}]_i$. For example, Ca^{2+}-dependent modulation of channel activity has

This article must therefore be hereby marked "advertisement" in accordance with 18 U.S.C. Section 1734 solely to indicate this fact.

K. Stroffekova (✉)
Department of Biology, Utah State University,
5305 Old Main Hill,
Logan, UT 84322-5305, USA
e-mail: stroffek@biology.usu.edu

been demonstrated for cyclic nucleotide-gated channels, *N*-methyl-D-aspartate receptors, ryanodine receptors (RyRs), inositol 1,4,5-triphosphate receptors, and high-voltage-activated Ca^{2+} channels [42, 32]. Many of these channels display Ca^{2+}-dependent modulation, either inactivation or facilitation (or both), that is mediated by calmodulin (CaM) [42].

The Ca_v1 family of channels contains four isoforms that exhibit distinct tissue-specific expression: $Ca_v1.1$ (skeletal muscle), $Ca_v1.2$ (cardiac myocytes and neurons), $Ca_v1.3$ (neurons and sino-atrial node cells), and $Ca_v1.4$ (retinal neurons). The Ca^{2+}-dependent modulation of $Ca_v1.2$ has been extensively studied; this channel displays Ca^{2+}-dependent inactivation (CDI) and facilitation (CDF), in addition to voltage-dependent inactivation [32, 37]. Both Ca^{2+}-dependent processes are mediated by CaM [37, 39, 47, 60]. The structural determinants of CDI have been assigned to the proximal region of the C terminus of $Ca_v1.2$ [4, 29, 61]. Three domains have been identified within this region: a Ca^{2+}-binding EF-hand motif, a CaM-tethering site, and a CaM-binding IQ motif (Fig. 1). The EF-hand motif, located ~16 residues beyond the end of the last transmembrane segment (IVS6), is absolutely necessary for CDI [37]. The CaM-tethering site, which consists of both $preIQ_3$ [16] and IQ motifs [35, 38], resides 50 amino acids downstream from the EF-hand motif and binds Ca^{2+}-free CaM (apo-CaM) at resting $[Ca^{2+}]_i$. The IQ motif resides downstream from the EF-hand motif and the pre-IQ_3 domain, and it binds Ca^{2+}-CaM [35, 43]. When interaction of CaM with either of these domains is compromised, CDI is reduced or eliminated.

The initial 200 amino acids of the C terminus of all members of the Ca_v1 family are highly conserved and contain the above-described domains (Fig. 1). However, there are striking differences in Ca^{2+} modulation between these different channel isoforms. For example, $Ca_v1.2$ mediates a fast-activating Ca^{2+} current that exhibits both fast CDI and CDF, $Ca_v1.3$ mediates a fast-activating Ca^{2+} current that displays fast CDI and slow CDI, and $Ca_v1.4$ mediates a fast-activating Ca^{2+} current that completely lacks CDI [33, 37, 59]. By contrast, $Ca_v1.1$ mediates a slowly activating Ca^{2+} current that does not display significant inactivation [57]. Whether $Ca_v1.1$ exhibits any form of Ca^{2+}-dependent modulation has been controversial [3, 22, 27]. In earlier studies, adult skeletal muscle fibers were used to investigate the underlying mechanism of inactivation of the skeletal L-type Ca^{2+} current [3, 22, 25]. Results from these studies led to two controversial explanations: (1) L-type Ca^{2+} current displays only slow voltage-dependent inactivation and no Ca^{2+}-dependent inactivation and (2) L-type Ca^{2+} current exhibits Ca^{2+}-dependent inactivation in addition to very slow voltage-dependent inactivation. However, the question of Ca^{2+}-dependent modulation of $Ca_v1.1$ has been difficult to address using adult skeletal muscle fibers because these cells possess an extensive transverse tubule system (TTS) and numerous ionic conductances.

In the present work, cultured mouse myotubes were used to explore the relationship between $Ca_v1.1$ and CaM. These cells are advantageous for this purpose because although they lack extensively invaginated TTS, the organization and position of $Ca_v1.1$ and RyR1 are the same as in adult fibers where $Ca_v1.1$ is organized in groups of four (tetrads), and each tetrad in T-tubules apposes every other RyR1 in junctional SR [20]. Importantly, the outward ionic currents in myotubes can be effectively blocked by appropriate internal and external solutions. Furthermore, cultured

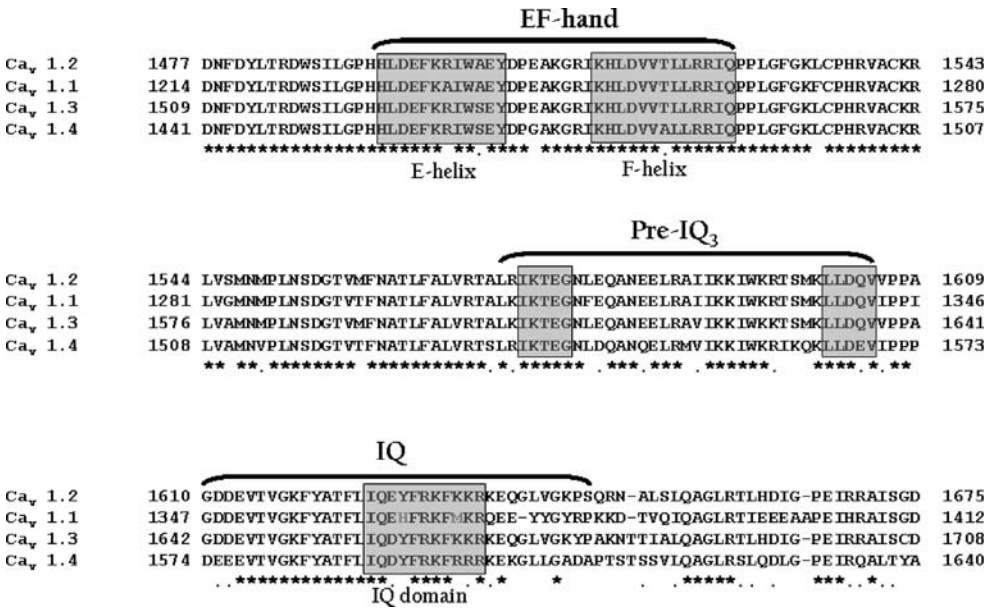

Fig. 1 Alignment of the proximal carboxyl termini of Ca_v1 family channels. The proximal 197 residues of each C terminus, beginning immediately downstream from the end of transmembrane segment IVS6, are compared. Sequences are from mouse $Ca_v1.2$ (Genbank accession number NM_009781), mouse $Ca_v1.1$ (XM_983862), rat $Ca_v1.3$ (NM_017298), and rat $Ca_v1.4$ (NM_053701)

myotubes can be made to express exogenous proteins through direct nuclear microinjection.

The results presented in this work demonstrate that $Ca_v1.1$ displays slow CDI that is mediated by CaM. Additionally, fluorescent resonance energy transfer (FRET) measurements show, for the first time, that CaM associates with $Ca_v1.1$ channel in vivo.

Experimental procedures

Molecular biology The coding sequences for rat wild-type CaM (CaM_{wt}) and rat mutant CaM incapable of binding Ca^{2+} (CaM_{1234}) were excised from their original vector (pcDNA3) [37] using *Xba*I and *Kpn*I and ligated into the multiple cloning site of *Xba*I- and *Kpn*I-digested EYFP-C1 (BD Biosciences Clontech, CA). All constructs were verified by restriction digest analysis and sequencing.

Electrophysiology Primary myotubes were cultured from normal newborn mouse skeletal muscle as previously described [52]. Approximately 1 week after plating, macroscopic Ca^{2+} currents were measured with the standard ruptured-patch whole-cell technique. In experiments assessing the effects of CaM on Ca^{2+} currents, normal myotubes (~1 week in culture) were injected with expression plasmids encoding CaM_{wt} or CaM_{1234} (gift of Dr. Yue [37]) and green fluorescent protein (pEGFP-C1, BD Biosciences Clontech) at concentrations of 0.7 and 0.02 μg/μl, respectively. Successfully transfected myotubes were identified 36–48 h after injection by their green fluorescence under UV illumination. Patch pipettes were constructed of borosilicate glass and had resistances of 1.8–2.5 MΩ when filled with the standard internal solution, which contained (in mM) 145 Cs-aspartate, 10 Cs_2-EGTA, 5 $MgCl_2$, and 10 HEPES (pH 7.4 with CsOH), or with BAPTA internal solution, in which 10 mM Cs_2-BAPTA replaced Cs_2-EGTA. The external solution contained (in mM) 145 tetraethylammonium chloride (TEA-Cl), 10 $CaCl_2$ or 10 $BaCl_2$, 0.03 tetrodotoxin, and 10 HEPES (pH 7.4 with TEA-OH). The holding potential was −80 mV, and test pulses were preceded by a 1-s prepulse to −30 mV to inactivate endogenous T-type Ca^{2+} currents. Recorded membrane currents were corrected off-line for linear components of leakage and capacitance by digitally scaling and subtracting the average of ten preceding control currents, elicited by hyperpolarizing voltage steps (30-mV amplitude) from the potential of −50 mV. Ca^{2+} currents were normalized by linear cell capacitance (expressed in pA/pF). Values for G_{max}, the maximal Ca^{2+} conductance, were obtained by fitting the measured currents according to the equation:

$$I_{peak} = G_{max}(V - V_R)/\{1 + \exp[-(V - V_{1/2})/k]\} \quad (1)$$

where I_{peak} is the peak current activated at the test potential V, V_R is the extrapolated reversal potential, $V_{1/2}$ is the potential for half-maximal activation of the Ca^{2+} conductance, and k is a slope factor. The fraction of current remaining at the end of an 800-ms test pulse was divided by the peak current ($r_{800}=I_{end}/I_{peak}$) and used to quantify the level of inactivation according to the equation:

$$\text{Inactivation } [\%] = (1 - r_{800}) \times 100\% \quad (2)$$

All recordings were performed at room temperature (~20°C), and data are reported as mean ± SEM; n indicates the number of myotubes tested. Data sets were statistically compared by an unpaired, two-sample Student's t test, with a confidence interval of at least 95%.

Confocal microscopy and FRET measurements Primary cultures of myotubes isolated from newborn dysgenic mice were plated onto 35-mm culture dishes with integral No. 0 glass coverslip bottoms (MatTek). Approximately 1 week after plating, myotubes were injected with expression plasmids encoding fluorescently tagged $Ca_v1.1$ (pECFP-$Ca_v1.1$; gift of Dr. K. Beam) and CaM (YFP-CaM). The rabbit skeletal muscle $Ca_v1.1$ was in CFP-C1 mammalian expression vector (BD Biosciences Clontech). Successfully transfected myotubes were identified 36–48 h after injection by their cyan or yellow fluorescence under UV illumination. Cells were bathed in rodent ringer (in mM: 146 NaCl, 5 KCL, 2 $CaCl_2$, 1 $MgCl_2$, 11 glucose, 10 HEPES; pH 7.4 adjusted with NaOH) and examined with an LSM 510 META laser scanning microscope (Zeiss, Thornwood, New York) with 40× oil objective. Two laser lines (458 and 514 nm) of the argon laser (30 mW maximum output, operated at 50% or 6.3 A), respectively, were used to excite CFP and YFP fluorophores. Emissions of CFP and YFP were recorded in multitrack configuration with a bandwidth filter of 465–495 nm (Chroma, Rockingham, VT, USA) and long-pass filter of 530 nm, respectively. Under these conditions, there is no cross-talk between the CFP and YFP fluorescence because CFP is not excited at 514 nm and YFP does not emit in the 465–495 nm range. To determine the magnitude of FRET, YFP-tagged CaM was photobleached by repeated (40–100) scans with the 514-nm line set at maximum laser intensity, which is 20- to 40-fold higher than the intensity used to elicit yellow fluorescence from YFP. Upon completion of YFP photobleaching, fluorescence intensities ($I_{CFPpost}$ and $I_{YFPpost}$) were recorded under the same conditions as before photobleaching. The increased emission of CFP-tagged $Ca_v1.1$ indicated that FRET had occurred between donor (CFP) and acceptor (YFP) fluorophores. Fluorescence intensities were analyzed by the 510 LSM Image Examiner and 3D Zeiss

software packages (Zeiss), and FRET efficiencies were calculated as:

$$E = \left(\frac{I_{\mathrm{CFPpost}} - I_{\mathrm{CFPpre}}}{I_{\mathrm{CFPpost}}}\right) \cdot 100\% \quad (3)$$

where I_{CFPpre} and I_{CFPpost} are the background-corrected CFP fluorescence intensities before and after photobleaching YFP, respectively.

Results

The native skeletal muscle L-type channel ($Ca_v1.1$) displays CDI Normal myotubes were used to test the hypothesis that endogenously expressed $Ca_v1.1$ exhibits CDI (Fig. 2). Whole-cell currents were evoked by 800-ms depolarizations, which was the longest duration test pulse that was experimentally compatible with stable recordings and myotube survival. During a depolarization of this length, Ca^{2+} currents mediated by $Ca_v1.1$ underwent significant

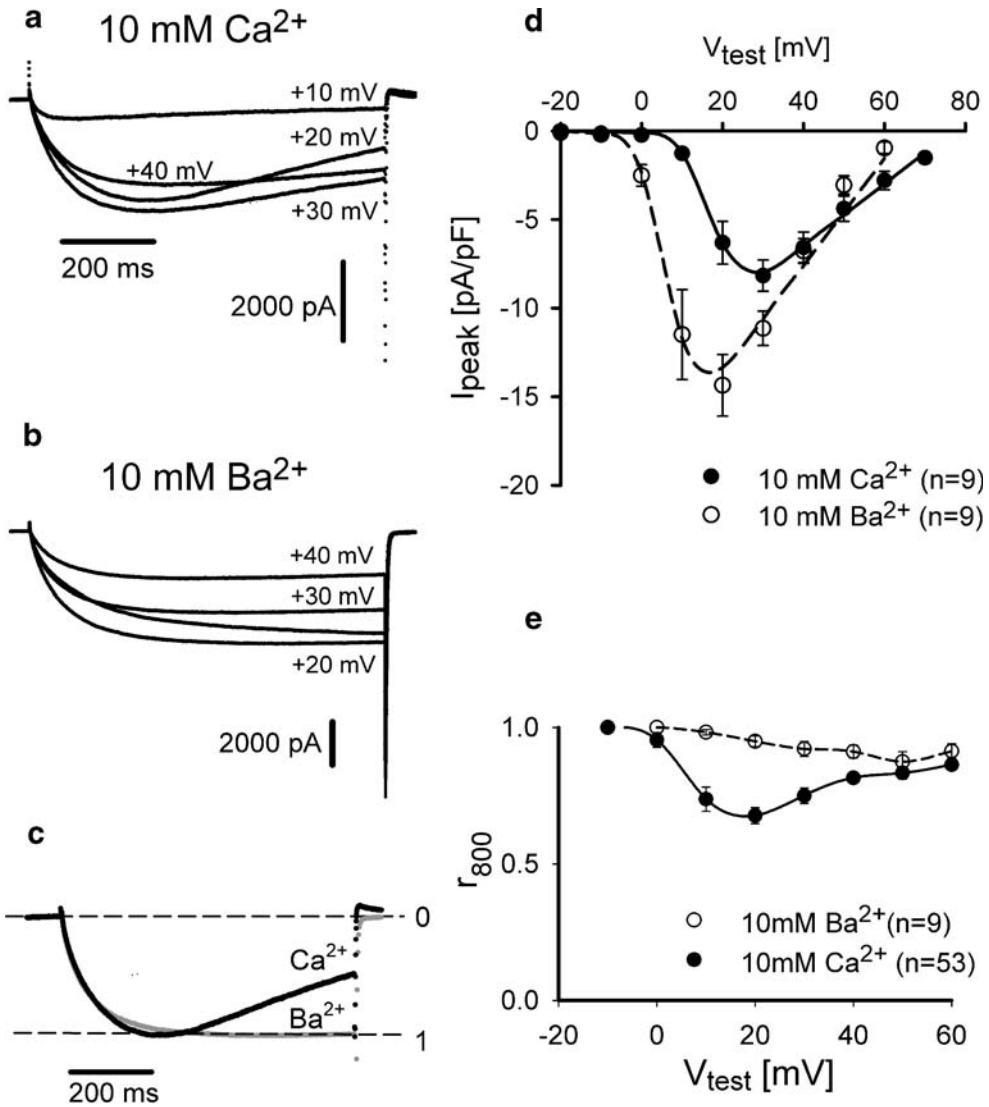

Fig. 2 Ba^{2+} virtually eliminates inactivation of $Ca_V1.1$ current. Representative whole-cell currents were recorded from normal myotubes using first Ca^{2+} (**a**) and then Ba^{2+} (**b**) as charge carrier. The currents shown in **a** and **b** were recorded from the same myotube [cell 4 (10–30–01); linear capacitance C=267 pF], initially using Ca^{2+} as charge carrier and then again after exchange of the external solution. Currents were elicited by 800-ms depolarizations to the indicated test potentials (+10 to +40 mV). Note that the scales are different for Ca^{2+} and Ba^{2+} currents. **c** The Ca^{2+} (*black trace*) and Ba^{2+} (*dark grey trace*) currents evoked by a depolarization to +20 mV in **a** and **b** were superimposed following normalization. **d** The average peak current density (I_{peak}) is plotted as a function of membrane potential (V_{test}). Data were obtained from the indicated number of myotubes for each group. The *smooth lines* through the data were generated by using the Eq. 1 ("Experimental procedures") and the average values. **e** The fraction of current remaining at the end of 800-ms depolarizations (r_{800}) is plotted as a function of test potential (V_{test}) for Ca^{2+} and Ba^{2+} currents recorded from normal myotubes. Symbols and error bars represent mean ± SEM, with the number of myotubes in parentheses

inactivation (Fig. 2a). The current remaining at the end of the pulse (r_{800}) displayed a U-shaped voltage-dependence (Fig. 2e, filled circles), consistent with a current-dependent inactivation process [7]. In such a process, the extent of inactivation varies in proportion to the amplitude of the inward calcium current, which in turn depends on the number of conducting channels and the electrochemical driving force on calcium. Test pulses to +10 mV and above elicited currents of sufficient amplitude to trigger current-dependent inactivation, as previously described for adult frog and mouse muscle fibers [3, 25] and heterologously expressed $Ca_v1.2$ and $Ca_v1.3$ [37, 59]. Inactivation was maximal at a test potential of +20 mV, as reflected by a minimum r_{800} value of 0.68±0.03 (n=53; Fig. 2e). Correspondingly, the Ca^{2+} current attained its maximum conductance at +20 mV (Fig. 2d and Table 1).

To investigate whether inactivation of $Ca_v1.1$ is ion specific as was previously shown for other Ca^{2+} channels [7, 8], currents were first recorded with 10-mM external Ca^{2+}; this solution was then replaced with one containing equimolar Ba^{2+} in place of Ca^{2+}, and whole-cell currents were again recorded in the same myotubes. Previous studies have shown that Ba^{2+} is ~100 times less effective than Ca^{2+} in triggering current-dependent inactivation of $Ca_v1.2$ [8, 19]. Exchange of Ba^{2+} for Ca^{2+} resulted in a significant increase in maximal ion conductance (from 239 to 383 nS/nF; p<0.02), a significant shift of about −11 mV (p<0.001) in the current/voltage (I–V) relationship, and the virtual elimination of inactivation. Altogether, inactivation was reduced from 30 to 2% at test potentials eliciting maximum currents (Table 1; Fig. 2b,d and e, open circles). These effects, which are similar to those observed for other L-type channels [8, 13, 54], indicate that inactivation of $Ca_v1.1$ is strongly dependent on Ca^{2+} permeation through the channel. Furthermore, the U-shaped voltage dependence of r_{800} when Ca^{2+} is the charge carrier (Fig. 2e) and the absence of inactivation when Ba^{2+} is the charge carrier indicate that $Ca_v1.1$ undergoes CDI.

Table 1 Ca^{2+} and Ba^{2+} conductances and their voltage-dependent characteristics in normal myotubes

Charge carrier ion	G_{max} (nS/nF)	V_R (mV)	$V_{1/2}$ (mV)	k (mV)	N
Ca^{2+}	233±27	69.6±3.15	19.7±1.3	3.8±0.3	9
Ba^{2+}	383±50**	60.3±2.2**	8.8±1.6*	4.3±0.4	9

Data are given as a mean ± SD where N is the number of myotubes tested. Values for G_{max}, the maximal Ca^{2+} conductance, were obtained by fitting the measured currents of each myotube according to Eq. 1 ("Experimental procedures"). All recordings were done at room temperature (~20°C). The data set for Ca^{2+} currents was compared statistically (unpaired, two-sample Student's t test) to the corresponding data set for Ba^{2+} currents in the same normal myotubes after exchange of the external solution. The confidence interval was 95% or greater. Statistical significance is indicated by single asterisk (p<0.001), and double asterisk (p<0.02).
*p<0.001
**p<0.02

In some of the myotubes, a small, slowly activating outward current was observed during 800-ms depolarizations, when Ca^{2+} currents were recorded with 10-mM external Ca^{2+} and 10-mM internal EGTA (Fig. 2a). This small outward current was eliminated when Ba^{2+} replaced external Ca^{2+} or when glutamate replaced external Cl^-, and it was also eliminated when BAPTA was substituted for EGTA in the pipette solution. Furthermore, addition of 0.2 mM niflumic acid (NiF), a known blocker of Ca^{2+}-activated Cl^- channels, to 10-mM external Ca^{2+} solution largely eliminated this small outward current, consistent with the possibility that this small outward current represents Cl^- influx through Ca^{2+}-activated Cl^- channels. Importantly, however, neither NiF nor replacement of external Cl^- with glutamate significantly affected the inactivation phenotype, i.e., the currents still displayed CDI and the U-shaped voltage dependence of r_{800} was preserved (data not shown).

CDI of $Ca_v1.1$ is sensitive to fast dynamic changes in $[Ca^{2+}]_i$ within the T-SR junction CDI of other members of the Ca_v1 family, as well as members of the Ca_v2 family, has been shown to be mediated by CaM. A model of Ca^{2+}-dependent modulation via CaM has been proposed for Ca_v1 and Ca_v2 families in which Ca^{2+} influx through the channel pore selectively activates the C-lobe of CaM, whereas more global increases in [Ca], for example those resulting from Ca^{2+} release from internal stores, preferentially activate the N-lobe of CaM [34]. Ca^{2+} binding to the N-lobe of CaM is prevented by the presence of Ca^{2+} buffers (either EGTA or BAPTA, at concentrations ranging from 1–10 mM), whereas Ca^{2+} binding to the C-lobe is not [32].

To assess whether CDI of $Ca_v1.1$ is affected by Ca^{2+} buffering, and thus indirectly investigate which lobe of CaM is responsible, Ca^{2+} currents were recorded from normal myotubes with either EGTA or BAPTA in the pipette solution. EGTA is a slow, high-affinity Ca^{2+} buffer that effectively buffers Ca^{2+} in the bulk myoplasm, but not in subcellular regions such as the T-SR junction (where $Ca_v1.1$ is localized) which experience fast dynamic changes in $[Ca^{2+}]$. In the presence of 10 mM EGTA, Ca^{2+} entering the T-SR junction can freely diffuse up to 140 nm before being bound by EGTA, which means that Ca^{2+} concentration can change dynamically by an order of magnitude within the T-SR junction. By contrast, 10 mM BAPTA is able to bind Ca^{2+} within 30 nm from the point of entry, thus BAPTA can effectively buffer Ca^{2+} concentration within the T-SR junction as well as within the bulk myoplasm [48, 50].

Figure 3 shows Ca^{2+} currents recorded from normal myotubes with either 10 mM EGTA or BAPTA in the

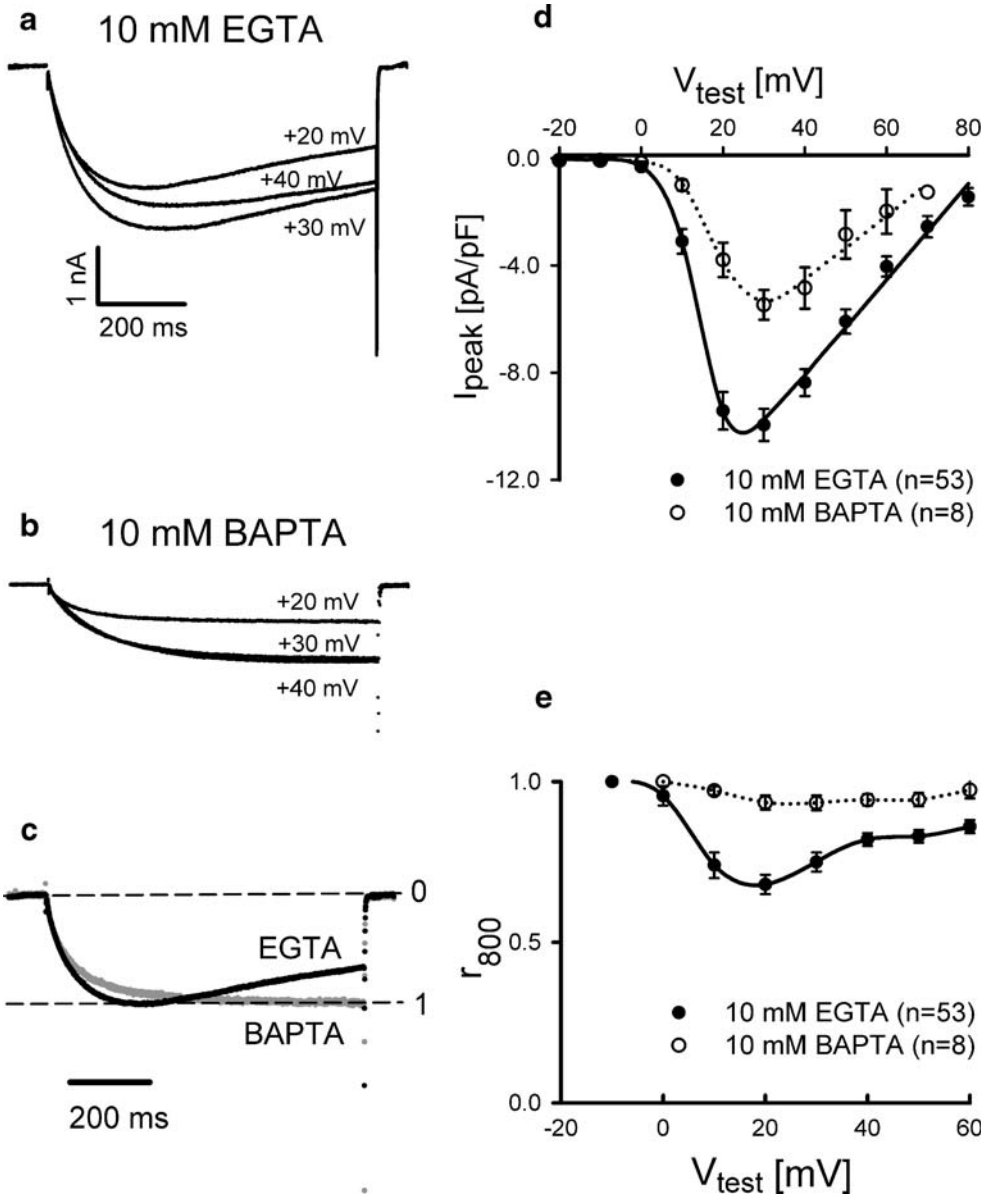

Fig. 3 Intracellular BAPTA eliminates CDI of $Ca_V1.1$. Representative whole-cell currents were recorded from normal myotubes with either 10 mM EGTA (**a**) or 10 mM BAPTA (**b**) in the pipette solution. Currents were elicited by 800-ms depolarizations to the indicated test potentials (+20 to +40 mV). **a** Cell 3 (11–5–01), C=250 pF; **b** cell 4 (9–11–03), C=254 pF. **c** Currents evoked at +20 mV with either EGTA (*black trace*) or BAPTA (*dark grey trace*) in the pipette solution were superimposed following normalization. These are the same +20-mV currents as illustrated in **a** and **b**. **d** The average peak current density (I_{peak}) is plotted as a function of membrane potential (V_{test}). Data were obtained from the indicated number of myotubes for each group. The *smooth lines* through the data were generated by using the Eq. 1 ("Experimental procedures") and the average values. **e** r_{800} values are plotted as a function of test potential (V_{test}) for Ca^{2+} currents recorded from normal myotubes using either EGTA or BAPTA in the pipette solution. Symbols and error bars represent mean ± SEM, with the number of myotubes in *parentheses*

pipette. Currents were recorded >5 min after achieving the whole-cell configuration to allow for adequate intracellular dialysis with the pipette solution. In the presence of EGTA, Ca^{2+} currents through $Ca_v1.1$ displayed a characteristic CDI (a, c, and e), indicating that EGTA does not prevent permeating Ca^{2+} from triggering CDI. By contrast, intracellular BAPTA virtually eliminated CDI and additionally produced significant changes in the I–V relationship. At test potentials that elicited maximal currents, r_{800} values were increased from 0.68±0.03 to 0.94±0.02 (p<0.001) in BAPTA-dialysed cells (Fig. 3b and e). The elimination of CDI by BAPTA suggests that intracellular accumulation of Ca^{2+} within the T-SR junction, or near the cytoplasmic mouth of the channel, is the trigger for CDI of $Ca_v1.1$. BAPTA also decreased the peak current density from −9.4 to −5.5 pA/pF (p<0.004). However, the maximal Ca^{2+} conductance was not significantly reduced (249±24 nS/nF with BAPTA, n=8 compared to 272±21 nS/nF with EGTA, n=53; Fig. 3d and Table 2), owing to a negative shift in the reversal potential (see below). Finally, BAPTA shifted the midpoint ($V_{1/2}$) of current activation by 6 mV (p<0.01), shifted the reversal potential (V_R) by −10.4 mV (p<0.02), and decreased the slope factor (k) by 1.4 mV (p<0.02; Table 2).

CaM mediates Ca^{2+}-dependent inactivation of skeletal L-type Ca^{2+} current The finding that $Ca_v1.1$ exhibits CDI in conjunction with the presence of a highly conserved CaM-interacting region within the C terminus of $Ca_v1.1$ prompted me to investigate whether CDI of $Ca_v1.1$ is mediated by CaM through a mechanism similar to that previously found for $Ca_v1.2$ and $Ca_v1.3$ [37, 44, 60]. One way to test for CaM involvement is to overexpress mutant

Table 2 Maximal Ca^{2+} conductance and its voltage-dependent characteristics recorded with either 10 mM EGTA or BAPTA as intracellular Ca^{2+} buffer

Ca^{2+} buffer	G_{max} (nS/nF)	V_R (mV)	$V_{1/2}$ (mV)	k (mV)	N
10 mM EGTA	272±21	75.6±1.7	17.7±1.0	3.8±0.2	53
10 mM BAPTA	249±24	65.2±3.5**	23.7±1.5*	5.2±0.4**	8

Data are given as a mean ± SD where N is the number of myotubes tested. Values for G_{max} were obtained by fitting the measured currents of each myotube according to Eq. 1 ("Experimental procedures"). All recordings were done at room temperature (~20°C). The data set for Ca^{2+} currents recorded with 10 mM EGTA in the pipette was compared statistically a corresponding set of Ca^{2+} currents recorded with 10 mM BAPTA in the pipette using an unpaired, two-sample Student's t test with a confidence interval of 95% or greater. Statistical significance is indicated by single asterisk ($p<0.01$) and double asterisk ($p<0.02$).
*$p<0.01$
**$p<0.02$

calmodulin (CaM_{1234}) that does not bind Ca^{2+}. CaM_{1234} has aspartate (D)-to-alanine (A) substitutions in all four EF-hand motifs to abolish Ca^{2+} binding [37]. Overexpression of CaM_{1234} produces a dominant negative effect that eliminates CDI of $Ca_v1.2$ and $Ca_v1.3$ [15, 16, 44, 59].

To test this approach, normal myotubes were injected with cDNAs encoding wild-type CaM (CaM_{wt}) or the mutant CaM_{1234}, and Ca^{2+} currents were recorded 48 h later. Skeletal muscle L-type Ca^{2+} currents recorded from myotubes overexpressing CaM_{wt} and CaM_{1234}, respectively, are shown in Fig. 4a and b. Overexpression of CaM_{wt} in normal myotubes did not significantly affect the *I–V* relationship (Fig. 4d and Table 3) or the extent of CDI compared to uninjected myotubes (Fig. 4e, half-filled squares), suggesting that the concentration of endogenous CaM is sufficient to fully populate native $Ca_v1.1$. However, in normal myotubes overexpressing CaM_{1234}, the extent of CDI was greatly suppressed (Fig. 4e, open diamonds), although the *I–V* relationship was unaffected (Fig. 4d and Table 3). On average, overexpression of CaM_{1234} significantly increased r_{800} from 0.68±0.03 to 0.92±0.02 (at a test potential of +20 mV; $p<0.01$), reflecting a large decrease in the extent of CDI. This result is similar to previous data obtained for $Ca_v1.2$ coexpressed with CaM_{1234} in HEK cells [37], and also for $Ca_v1.2$ and CaM_{1234} coexpressed in dysgenic myotubes, where the r_{800} increased from 0.7 to 0.9 in comparison with myotubes expressing $Ca_v1.2$ alone [51]. Altogether, these results indicate that CaM mediates CDI of $Ca_v1.1$.

CaM associates with $Ca_v1.1$ in vivo It has been shown that CaM is tethered to $Ca_v1.2$ in the Ca^{2+}-free form (apo-CaM) and functions as the Ca^{2+} sensor for CDI. The CaM-tethering site binds apo-CaM and consists of two short peptide sequences ($preIQ_3$ and IQ motifs [14]), and these sequences are conserved in $Ca_v1.1$ (Fig. 1). To date, only in vitro approaches have been used to investigate potential interactions between $Ca_v1.1$ and CaM [35, 43]. No previous studies have tested for in vivo association of CaM with $Ca_v1.1$.

To examine this issue, confocal microscopy and FRET were used to test whether $Ca_v1.1$ and CaM interact in vivo. The FRET method is an appropriate tool for analyzing the relative position of donor and acceptor fluorophores that are separated by distances of 10 nm or less; such distances are relevant to protein–protein interactions in vivo [14], and FRET has been used for determining the in vivo association of $Ca_v1.2$ and CaM [15, 16]. The efficiency of FRET between CFP-$Ca_v1.1$ and YFP-CaM_{wt} was determined by means of acceptor photobleaching ("Experimental procedures"). Figure 5 shows confocal images of *cyan* and *yellow* fluorescence from a dysgenic myotube expressing both CFP-$Ca_v1.1$ and YFP-CaM_{wt}. Expression of CFP-$Ca_v1.1$ resulted in the appearance of small cyan fluorescence foci located near the cell surface. The small foci correspond to groups of $Ca_v1.1$ localized to T-SR junctions; these foci are similar in size and distribution to those of $Ca_v1.1$ foci revealed by immunohistochemistry [21]. Expression of YFP-CaM resulted in the appearance of homogeneous *yellow* fluorescence, as CaM is a cytoplasmic protein. Panel a shows emission of *cyan* and *yellow* fluorescence before photobleaching. Panel b shows the same cell after acceptor (YFP) photobleaching. After photobleaching YFP-CaM_{wt}, there was a notable increase in the cyan signal from foci. FRET efficiency (E) was determined according to Eq. 3 (see "Experimental procedures") and was found to have a value of E=12%. Overall, seven cells were examined, and the average FRET efficiency was estimated as E=4.06±1.11% (n=7). For comparison, the FRET efficiency between $Ca_v1.2$-CFP and CaM_{wt}-YFP coexpressed in HEK293 cells was estimated as E=10±1.1% (n=8) [16]. It should be noted that the FRET signal between $Ca_v1.2$ and CaM_{wt} is stronger due to the position of the donor fluorophore at the C terminus of $Ca_v1.2$, whereas in the present experiment, the donor fluorophore was positioned at the N terminus of $Ca_v1.1$, and the fluorophores were thus farther apart. Despite the N-terminal location of CFP in the present experiments, the measured FRET signal between CFP-$Ca_v1.1$ and YFP-CaM_{wt} in dysgenic myotubes is highly relevant, and it strongly suggests that CaM associates with $Ca_v1.1$ in vivo.

Discussion

The present study provides new information about the skeletal muscle L-type Ca^{2+} channel ($Ca_v1.1$). Specifically,

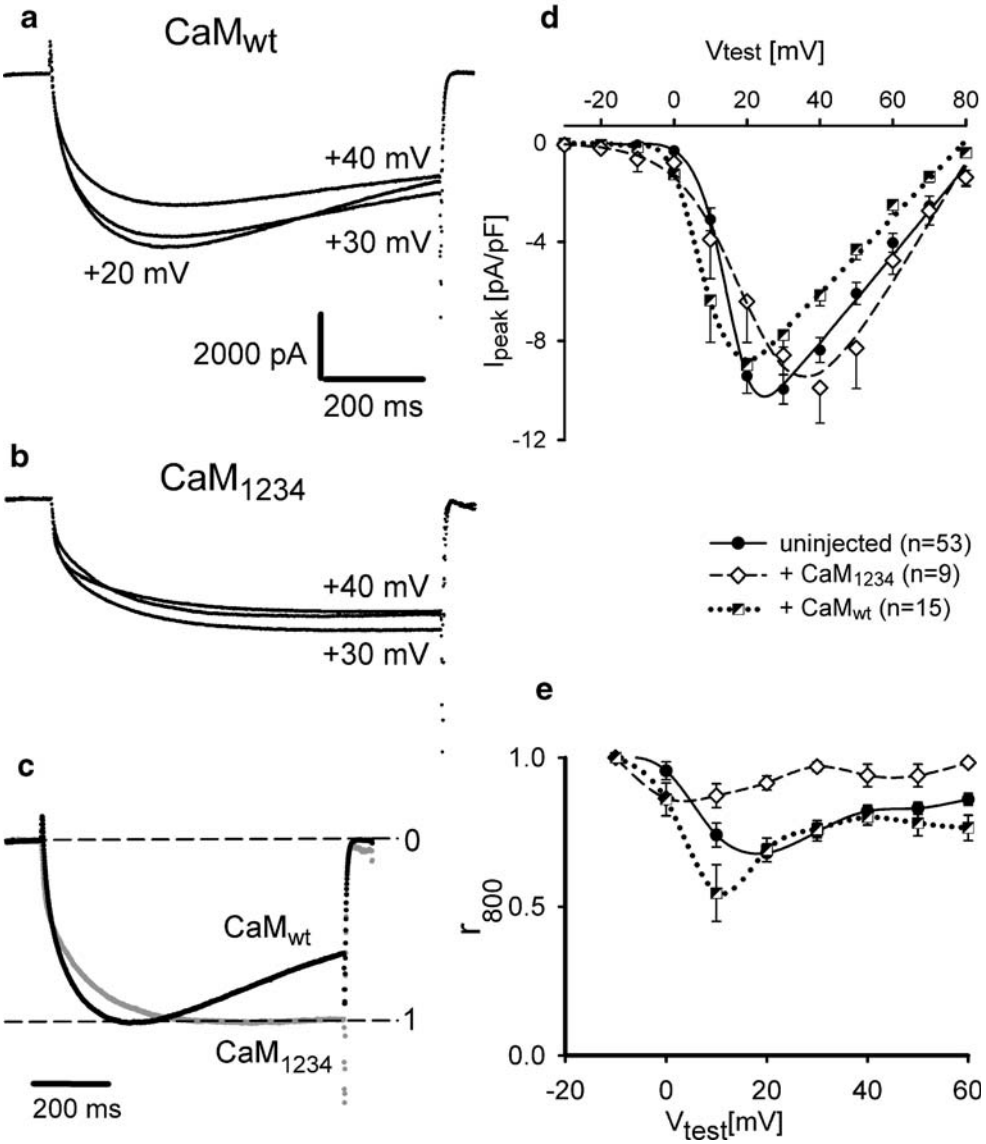

Fig. 4 CaM mediates CDI of $Ca_v1.1$. Representative Ca^{2+} currents recorded from normal myotubes that overexpressed either CaM_{wt} (**a**) or CaM_{1234} (**b**). Currents were elicited by 800-ms depolarizations from −80 mV to the indicated test potentials (+20 to +40 mV). **a** Cell 3 (6–26–02), C=813 pF; **b** cell 1 (2–5–02), C=343 pF. **c** Currents recorded at +20 mV from myotubes overexpressing either CaM_{wt} (*black trace*; from **a**) or CaM_{1234} (*grey trace*; from **b**) were superimposed following normalization. **d** The average peak current density (I_{peak}) is plotted as a function of membrane potential (V_{test}). Data were obtained from the indicated number of myotubes for each group. The *smooth lines* through the data were generated by using the Eq. 1 ("Experimental procedures") and the average values. **e** r_{800} values are plotted as a function of test potential (V_{test}) for Ca^{2+} currents recorded from uninjected myotubes and myotubes overexpressing CaM_{wt} or CaM_{1234}. Symbols and error bars represent mean ± SEM, with the number of myotubes in *parentheses*

Table 3 Ca^{2+} conductance and its voltage-dependent characteristics in normal myotubes overexpressing CaM_{wt} or CaM_{1234}

Treatment	G_{max} (nS/nF)	V_R (mV)	$V_{1/2}$ (mV)	k (mV)	N
Uninjected	272±21	75.6±1.7	17.7±1.0	3.8±0.2	53
+CaM_{wt}	221±18.61	83.04±3.06	14.42±2.33	2.8±0.33	15
+CaM_{1234}	245±35.97	80.05±3.55	19.95±2.48	3.81±0.46	9

Data are given as a mean ± SD where N is the number of myotubes tested. Values for G_{max} were obtained by fitting the measured currents of each myotube according to Eq. 1 ("Experimental procedures"). All recordings were done at room temperature (~20°C). The data sets for myotubes overexpressing CaM_{wt} or CaM_{1234} were separately compared to the corresponding data set from uninjected myotubes using an unpaired, two-sample Student's t test with a confidence interval of 95% or greater.

the data demonstrate, for the first time, that $Ca_v1.1$ undergoes Ca^{2+}-dependent inactivation that requires CaM. Additionally, the results show that CaM associates with $Ca_v1.1$ in vivo.

The skeletal muscle L-type Ca^{2+} current has been extensively studied in adult amphibian and mammalian muscle fibers [3, 9–13, 17, 18, 22, 24, 25, 27], and several of these studies have investigated the mechanisms underlying inactivation. In general, these studies have concluded either that $Ca_v1.1$ displays only voltage-dependent inactivation [9, 27] or, alternatively, that $Ca_v1.1$ exhibits both Ca^{2+}-dependent and voltage-dependent inactivation [3, 24]. However, whether $Ca_v1.1$ exhibits CDI has remained unresolved.

The present experiments demonstrate that natively expressed $Ca_v1.1$ displays classic features of CDI, includ-

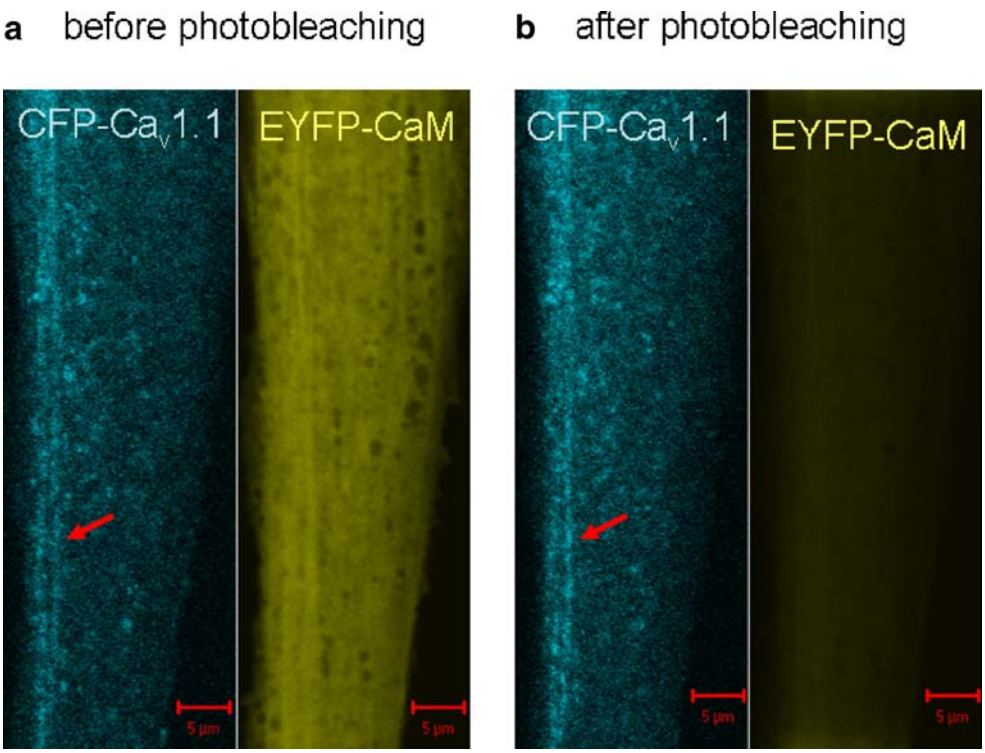

Fig. 5 FRET measurements indicate that $Ca_v1.1$ interacts with CaM_{wt} in vivo. CFP-$Ca_v1.1$ and YFP-CaM_{wt} were coexpressed in dysgenic myotubes. Confocal microscopy was used to measure the intensities of *cyan* and *yellow* fluorescence both before (**a**) and after (**b**) photobleaching the acceptor fluorophore (EYFP-CaM). Before and after measurements were obtained from the same myotube. The *cyan* fluorescence signal was significantly increased after photobleaching the acceptor, indicating the presence of significant FRET. Note that cyan fluorescence appears as small foci (*arrows*). The efficiency of FRET (*E*) was determined according to Eq. 3 (see "Experimental procedures") and had a value of E=12% for the myotube shown in this figure. The scale bar corresponds to 5 µm

ing U-shaped voltage dependence and elimination of inactivation when Ba^{2+} replaces Ca^{2+} as charge carrier or when the fast Ca^{2+} buffer BAPTA is present intracellularly. The U-shaped voltage dependence indicates that inactivation is current dependent and is greatest at potentials eliciting the greatest inward Ca^{2+} current. Ba^{2+} is widely used as a charge carrier in studies of Ca^{2+} channel function, and it is generally accepted that Ba^{2+} cannot effectively activate the Ca^{2+}-binding sites of Ca^{2+}-activated proteins such as CaM. Thus, it is generally assumed that voltage-gated Ca^{2+} channels exhibit only voltage-dependent inactivation when Ba^{2+} is used as the charge carrier [37, 44]. However, this is not strictly true, as Ba^{2+} currents mediated by $Ca_v1.2$ display both current-dependent and voltage-dependent inactivation, although it is important to note that the affinity of Ba^{2+} for the "inactivation site" on the $Ca_v1.2$ channel is 100-fold lower than that of Ca^{2+} [19]. The ability of BAPTA to eliminate CDI of $Ca_v1.1$ suggests that CDI is triggered by accumulation of Ca^{2+} within the T-SR junction.

This study was performed on primary cultures of skeletal muscle myotubes, which provide a natural cellular environment for $Ca_v1.1$. It is important to recognize that myotubes differ morphologically from adult skeletal muscle fibers. Myotubes grown in culture for 6–7 days, like those employed here, possess fully developed sarcomeric organization and distinct SR and T tubular systems (TTS) [20, 23], and the mechanism of skeletal muscle-type EC coupling appears to be functionally mature in such cells [49]. Importantly, myotubes differ from adult fibers by the fact that in myotubes, most (~88%) of the T-tubules are oriented longitudinally and do not penetrate very far into the cell's interior [20, 23]. Thus, T-SR junctions are located close to the myotube's surface, and the diffusion of extracellular ions to the junction is relatively unrestricted, in contrast to the situation which exists in adult fibers. Consequently, Ca^{2+} depletion within the TTS, which has been suggested to contribute to inactivation of the L-type current in adult fibers [3], is unlikely to play a significant role in CDI of $Ca_v1.1$ in myotubes.

One interesting finding of the present study is that CDI of $Ca_v1.1$ is considerably slower (τ_i~500 ms) than the previously reported "fast" CDI of $Ca_v1.2$ and $Ca_v1.3$ (τ_i~20 ms), which was shown to be triggered by Ca^{2+} binding to the C-lobe of CaM [37, 44]. The mechanism underlying the relative slowness of CDI by $Ca_v1.1$ remains to be determined. However, it may be a consequence of the slow activation rate of $Ca_v1.1$, as channel activation and inactivation are interdependent processes [28]. $Ca_v1.1$ activates at least tenfold slower than other members of the Ca_v1 family. For instance, at room temperature, $Ca_v1.1$ activates with a time constant (τ_a) of ~20–200 ms, whereas $Ca_v1.2$ activates with a τ_a of ~2 ms [56]. Alternatively, the relatively slow CDI of $Ca_v1.1$ may reflect a different underlying mechanism than that which underlies fast CDI of $Ca_v1.2$. The speed at which $Ca_V1.1$ undergoes CDI is very similar to the "slow" CDI of $Ca_v1.3$ (τ_i~400 ms;

estimated from Fig. 2 of [58], which was previously shown to be triggered by Ca^{2+} binding to N-lobe of CaM [37, 44]. This similarity suggests that CDI of $Ca_v1.1$ may also be triggered by Ca^{2+} binding to N-lobe of CaM, according to a model proposed for Ca^{2+}/CaM-dependent regulation of Ca_v1 and Ca_v2 family channels [32]. Further experiments (currently in progress) will be needed to test this possibility.

The results obtained with CaM_{1234} (Fig. 4) demonstrate that CaM is required for CDI of $Ca_v1.1$. This demonstration suggests that the general mechanism of CDI may be similar for all channels of the Ca_v1 and Ca_v2 families. Consistent with this possibility, the structural determinants of CaM-dependent CDI have been identified within the proximal C terminus of the Ca_v subunit, and these determinants are conserved among all members of the Ca_v1 and Ca_v2 families [4, 29, 60]. Previously, information concerning the interaction between $Ca_v1.1$ and CaM has been limited to in vitro experiments. For example, it has been reported that the $preIQ_3$ and IQ motifs of $Ca_v1.1$ can bind apo-CaM and Ca-CaM, respectively, in a fashion similar to the corresponding domains of $Ca_v1.2$ [35, 43]. The present results with overexpression of CaM_{1234} in normal myotubes (Fig. 4) are the first to indicate that CaM modulates the function of $Ca_v1.1$ in vivo. Furthermore, the significant FRET signal detected between CFP-$Ca_v1.1$ and YFP-CaM_{wt} in dysgenic myotubes (Fig. 5) provides the first indication that CaM associates with $Ca_v1.1$ in vivo.

Intracellular BAPTA produced significant effects on some of the biophysical properties of macroscopic $Ca_v1.1$ currents (Fig. 3). For example, BAPTA decreased the peak current density, shifted the *I–V* relationship to more positive potentials, shifted the reversal potential to more negative potentials, and decreased the slope factor (k) of the conductance–voltage relationship. These results are consistent with a previous study in which the presence of 5 mM BAPTA plus 0.5 mM $CaCl_2$ shifted activation of the *I–V* relationship by approximately +6 mV [31]. Additionally, in dialyzed adult frog skeletal muscle fibers, the presence of 20 mM BAPTA resulted in a significant decrease in the maximum quantity of intramembrane charge movement (Q_{max}), which reflects the activity of the voltage-sensors for EC coupling [49]. Charge movement is an intramembrane current caused by the voltage-dependent movement of charged S4 segments within each transmembrane domain of $Ca_v1.1$, and the "ON" charge movement in response to depolarization precedes the onset of inward L-type Ca^{2+} current [28]. Furthermore, L-type Ca^{2+} currents have been reported to "run down" more rapidly in the presence of intracellular BAPTA [18, 26]. These effects of BAPTA may indicate that dynamic changes in Ca^{2+} concentration within the T-SR junction play a role in voltage-sensing by $Ca_v1.1$. It is conceivable that, when BAPTA is present in the intracellular environment of myotube or adult muscle fiber, the voltage sensed by $Ca_v1.1$ is altered. In this regard, it has been demonstrated that Ca^{2+}-free BAPTA can penetrate into the lipid bilayer and remove Ca^{2+} from either extracellular or intracellular face, thereby reducing the negative charge screening effect of Ca^{2+} and changing the electric field across the membrane [41]. Alternatively, BAPTA may produce additional effects on channel function that are independent of its Ca^{2+}-buffering properties. This possibility is suggested by previous studies of slow muscarinic inhibition of Ca_v channels showing that BAPTA disrupts channel modulation via a mechanism independent of Ca^{2+} buffering [5, 6].

Despite decades of study, the physiological significance of the skeletal muscle L-type Ca^{2+} current has remained unclear. Single contractions of skeletal muscle fibers do not require Ca^{2+} current through $Ca_v1.1$ because skeletal muscle-type EC coupling is mediated by a mechanical interaction between the voltage sensor for EC coupling (i.e., $Ca_v1.1$) and the Ca^{2+} release channels of the SR [45, 40]. Thus, skeletal muscle fibers produce normal twitches in the temporary absence of external Ca^{2+}. However, during sustained or repetitive contractions, Ca^{2+} current through $Ca_v1.1$ may be necessary for maintaining force [30, 46]. The mechanism underlying regulation of contractile force by external Ca^{2+} is unknown. It is conceivable that Ca^{2+} entry can enhance contraction directly, or entering Ca^{2+} may be sequestered into the SR and thereby increase the amount of Ca^{2+} available for release in response to subsequent action potentials, which would lead to an increase in contractile force. Furthermore, during repetitive EC coupling in rat and frog skeletal muscle fibers, the resultant increase in intracellular [Ca^{2+}] triggers a significant increase in Q_{max}, suggesting a potential physiological role for Ca^{2+} influx in regulating the voltage-sensor function of $Ca_v1.1$ [11, 17, 49, 50]. Finally, in skeletal muscle fibers of aged mice and humans, the L-type Ca^{2+} current through $Ca_v1.1$ seems to play an important role both in EC coupling and in maintaining contractile force [12, 36]. Because normal daily activities require sustained activation of skeletal muscles, Ca^{2+} influx through $Ca_v1.1$ should play an important role. Ca^{2+}-dependent inactivation of $Ca_v1.1$ may thus represent an important mechanism for fine-tuning regulation of intracellular [Ca^{2+}] and consequently of skeletal muscle function.

Acknowledgment I thank Dr. David Yue for kindly providing CaM_{wt} and CaM_{1234} constructs, Dr. Kurt Beam for fruitful discussion, providing CFP-Ca_v 1.1 construct, and for his support of preliminary studies, and Dr. Brett Adams for his helpful insights and constructive criticism of the manuscript. This work was supported by MDA Research Grant (to K.S.). The costs of publication of this article were defrayed in part by the payment of page charges.

References

1. Armstrong CM, Bezanilla F, Horowicz P (1972) Twitches in the presence of ethyleneglycol-bis(β-aminoethylether)-*N*-*N*'-tetraacetic acid. Biochem Biophys Acta 267:605–608
2. Adams B, Beam KG (1990) Muscular dysgenesis in mice: a model system for studying excitation-contraction coupling. FASEB J 4:2809–2816
3. Almers W, Fink R, Palade PT (1981) Calcium depletion in frog muscle tubules: The decline of calcium current under maintained depolarization. J Physiol 312:177–207
4. Babitch J (1990) Channel hands. Nature 346:321–322
5. Bannister RA, Melliti K, Adams BA (2002) Reconstituted slow muscarinic inhibition of neuronal ($Ca_v1.2c$) L-Type Ca^{2+} channels. Biophys J 83:3256–3267
6. Beech DJ, Bernheim L, Mathie A, Hille B (1991) Intracellular Ca^{2+} buffers disrupt muscarinic suppression of Ca^{2+} current and M current in rat sympathetic neurons. Proc Natl Acad Sci USA 88:652–656
7. Brehm P, Eckert R (1978) Calcium entry leads to inactivation of calcium channel in Paramecium. Science 202:1203–1206
8. Chad JE, Eckert R (1986) An enzymatic mechanism for calcium current inactivation in dialysed Helix neurons. J Physiol 378:31–51
9. Cota G, Stefani E (1989) Voltage-dependent inactivation of slow calcium channels in intact twitch muscle fibers of the frog. J Gen Physiol 94:937–951
10. Delbono O (1992) Calcium current activation and charge movement in denervated mammalian skeletal muscle fibres. J Physiol 451:187–203
11. Delbono O, Stefani E (1993) Calcium current inactivation in denervated mammalian skeletal muscle fibres. J Physiol 460:173–183
12. Delbono O, O'Rourke KS, Ettinger WH (1995) Excitation-calcium release uncoupling in aged single human skeletal muscle fibers. J Membrane Biol 148:211–222
13. Donaldson PL, Beam KG (1983) Calcium currents in a fast-twitch skeletal muscle of the rat. J Gen Physiol 82:449–468
14. dos Remedios CG, Moens PD (1995) Cofilin, actin and their complex observed in vivo using fluorescence resonance energy transfer. J Struct Biol 115:175–185
15. Erickson MG, Alseikhan BA, Peterson BZ, Yue DT (2001) Preassociation of calmodulin with voltage-gated Ca^{2+} channels revealed by FRET in single living cells. Neuron 31:973–985
16. Erickson MG, Liang H, Mori MX, Yue DT (2003) FRET two-hybrid mapping reveals function and location of L-type Ca^{2+} channel CaM preassociation. Neuron 39:97–107
17. Feldmeyer D, Melzer W, Pohl B, Zöllner P (1992) Modulation of calcium current gating in frog muscle by conditioning depolarization. J Physiol 457:639–653
18. Feldmeyer D, Melzer W, Pohl B, Zöllner P (1993) A possible role of sarcoplasmic Ca^{2+} release in modulating the slow Ca^{2+} current of skeletal muscle. Pflűg Arch 425:54–61
19. Ferreira G, Yi J, Rios E, Shirokov R (1997) Ion-dependent inactivation of barium current through L-type calcium channels. J Gen Physiol 109:449–461
20. Flücher BE, Phillips JL, Powell JA, Andrews SB, Daniels MP (1992) Coordinated development of myofibrils, sarcoplasmic reticulum and transverse tubules in normal and dysgenic mouse skeletal muscle, in vivo and in vitro. Develop Biol 150:266–280
21. Flucher BE, Kasielke N, Grabner M (2000) The triad targeting signal of the skeletal muscle calcium channel is localized in the COOH terminus of the α_{1S} subunit. J Cell Biol 151:467–478
22. Francini F, Stefani E (1989) Decay of the slow calcium current in twitch muscle fibers of the frog is influenced by intracellular EGTA. J Gen Physiol 94:953–969
23. Franzini-Armstrong C (1991) Simultaneous maturation of transverse tubules and sarcoplasmic reticulum during muscle differentiation in the mouse. Develop Biol 146:353–363
24. Friedrich O, Ehmer T, Fink RHA (1999) Calcium currents during contraction and shortening in enzymatically isolated murine skeletal muscle fibres. J Physiol 517:757–770
25. Garcia J, McKinley K, Appel SH, Stefani E (1992) Ca^{2+} current and charge movement in adult single human skeletal muscle fibres. J Physiol 454:183–196
26. Grabner M, Dirksen RT, Suda N, Beam KG (1999) The II-III loop of the skeletal muscle dihydropyridine receptor is responsible for the bi-directional coupling with the ryanodine receptor. J Biol Chem 274:21913–21919
27. Harasztosi Cs, Sipos I, Kovacs L, Melzer W (1999) Kinetics of inactivation and restoration from inactivation of the L-type calcium current in human myotubes. J Physiol 516:129–138
28. Hille B (2001) Ion channels of excitable membranes, 3rd edn. Sinauer Assoc, Inc., Sunderland, MA
29. Imredy JP, Yue DT (1994) Mechanism of Ca^{2+}-sensitive inactivation of L-type Ca^{2+} channels. Neuron 12:1301–1318
30. Kotsias BA, Muchnik S, Obejero-Paz CA (1986) Co^{2+}, low Ca^{2+}, and verapamil reduce mechanical activity in rat skeletal muscles. Am J Physiol 250:C40–C46
31. Köhr G, Mody I (1991) Endogenous intracellular calcium buffering and the activation/inactivation of HVA calcium currents in rat dentate gyrus granule cells. J Gen Physiol 98:941–967
32. Liang H, DeMaria CD, Erickson MG, Mori MX, Alseikhan BA, Yue DT (2003) Unified mechanism of Ca^{2+} regulation across Ca^{2+} channel family. Neuron 39:951–960
33. McRory JE, Hamid J, Doering CJ, Garcia E, Parker R, Hamming K, Chen L, Hildebrand M, Beedle AM, Feldcamp L, Zamponi GW, Snutch TP (2004) The *CACNA1F* gene encodes an L-type calcium channel with unique biophysical properties and tissue distribution. J Neurosci 24(7):1707–1718
34. Melzer W, Herrman-Frank A, Lüttgau HCh (1995) The role of Ca^{2+} ions in excitation–contraction coupling of skeletal muscle fibres. Bioch Biophys Acta 1241:59–116
35. Pate P, Mochca-Morales J, Wu Y, Zhang J, Rodney GG, Serysheva II, Williams BY, Anderson ME, Hamilton SL (2000) Determinants for calmodulin binding on voltage-dependent Ca^{2+} channels. J Biol Chem 275:39786–39792
36. Payne AM, Zheng Z, Gonzales E, Wang ZM, Messi ML, Delbono O (2004) External Ca^{2+}-dependent excitation-contraction coupling in a population of ageing mouse skeletal muscle fibres. J Physiol 560:137–155
37. Peterson BZ, DeMaria CD, Yue DT (1999) Calmodulin is the sensor for Ca^{2+}-dependent inactivation of L-type calcium channels. Neuron 22:549–558
38. Pitt GS, Zühlke RD, Hudmon A, Schulman H, Reuter H, Tsien RW (2001) Molecular basis of calmodulin tethering and Ca^{2+}-dependent inactivation of L-type Ca^{2+} channels. J Biol Chem 276:30794–30802
39. Qin N, Olcesse R, Bransby M, Lin T, Birnbaumer L (1999) Ca^{2+}-induced inhibition of the cardiac Ca^{2+} channel depends on calmodulin. Proc Natl Acad USA 96:2435–2438
40. Rios E, Brum G (1987) Involvement of dihydropyridine receptors in excitation–contraction coupling in skeletal muscle. Nature 325:717–720
41. Rousset M, Cens T, Van Mau N, Charnet P (2004) Ca^{2+}-dependent interaction of BAPTA with phospholipids. FEBS Lett 576:41–45
42. Saimi Y, Kung Ch (2002) Calmodulin as an ion channel subunit. Annu Rev Physiol 64:289–311
43. Sencer S, Papineni RVL, Halling DB, Pate P, Krol J, Zhang J, Hamilton SL (2001) Coupling of RyR1 and L-type calcium

channels via calmodulin binding domains. J Biol Chem 276:38237–38241
44. Shen Y, Yu D, Hiel H, Liao P, Yue DT, Fuchs PA, Soong TW (2006) Alternative splicing of the Ca_v 1.3 channel IQ domain, a molecular switch for Ca^{2+}-dependent inactivation within auditory hair cells. J Neurosci 26(42):10690–10699
45. Schneider MF, Chandler WK (1973) Voltage dependent charge movement in skeletal muscle: a possible step in excitation-contraction coupling. Nature (London) 242:244–246
46. Sculptoreanu A, Scheuer T, Catterall WA (1993) Voltage-dependent potentiation of L-type Ca^{2+} channels due to phosphorylation by cAMP-dependent protein kinase. Nature 364:240–243
47. Soldatov NM, Oz M, O'Brien KA, Abernethy DR, Morad M (1998) Molecular determinants of L-type Ca^{2+} channel inactivation. J Biol Chem 273:957–963
48. Stern MD (1992) Buffering of calcium in the vicinity of a channel pore. Cell Calcium 13:183–192
49. Stroffekova K, Heiny JA (1997a) Triadic Ca^{2+} modulates charge movement in skeletal muscle. Gen Physiol Biophys 16:59–77
50. Stroffekova K, Heiny JA (1997b) Stimulation-dependent redistribution of charge movement between unavailable and available states. Gen Physiol Biophys 16:79–89
51. Stroffekova K, Yue DT, Beam KG (2001a) (2793-Pos) The effect of calmodulin on cardiac and skeletal L-type Ca^{2+} currents in skeletal muscle myotubes. Biophys J 80:2793-Pos
52. Stroffekova K, Proenza C, Beam KG (2001b) The protein-labeling reagent FLASH-EDT_2 binds not only to CCXXCC motifs but also non-specifically to endogenous cysteine-rich proteins. Pflügers Arch 442:859–866
53. Schwartz LM, McCleskey EW, Almers W (1985) Dihydropyridine receptors in muscle are voltage-dependent but most are not functional calcium channels. Nature 314:7470–7751
54. Tanabe T, Beam KG, Powell JA, Numa S (1988) Restoration of excitation–contraction coupling and slow calcium current in dysgenic muscle by dihydropyridine receptor complementary DNA. Nature 336:134–1395
55. Tanabe T Beam KG, Adams BA, Niidome T, Numa S (1990a) Regions of the skeletal muscle dihydropyridine receptor critical for excitation-contraction coupling. Nature 346:567–569
56. Tanabe T, Mikami A, Numa S, Beam KG (1990b) Cardiac-type excitation-contraction coupling in dysgenic skeletal muscle injected with cardiac dihydropyridine receptor cDNA. Nature 344:451–453
57. Tanabe T, Adams BA, Numa S, Beam KG (1991) Repeat I of the dihydropyridine receptor is critical in determining calcium channel activation kinetics. Nature 352:800–803
58. Wahl-Schott C, Baumann L, Cuny H, Eckert C, Griessmeier K, Biel M (2006) Switching off calcium-dependent inactivation in L-type calcium channels by an autoinhibitory domain. PNAS 103:15657–15662
59. Yang PS, Alseikhan BA, Hiel H, Grant L, Mori MX, Yang W, Fuchs PA, Yue DT (2006) Switching of Ca^{2+}-dependent inactivation of Ca_v 1.3 channels by calcium binding proteins of auditory hair cells. J Neuroscience 26(42):10677–10689
60. Zühlke RD, Reuter H (1998) Ca^{2+}-sensitive inactivation of L-type channels depends on multiple cytoplasmic amino acid sequences of the α_{1C} subunit. Proc Natl Acad Sci USA 95:3287–3294
61. Zühlke RD, Pitt GS, Deisseroth K, Tsien RW, Reuter H (1999) Calmodulin supports both inactivation and facilitation of L-type calcium channels. Nature 399:159–162